

RESEARCH

Open Access



Rheological properties of binary mixtures of *Lepidium perfoliatum* seed gum and xanthan gum

Alireza Yousefi^{1*}, Komla Ako², Ghader Hosseinzadeh¹ and Shahla Khodabakhshaghdam¹

Abstract

Background In this work, viscoelasticity, flow behaviour, thixotropy and thermo-rheological properties of binary mixtures of *Lepidium perfoliatum* seed gum (LPSG), as an emerging food gum, and xanthan gum (XG) at various blending ratios of 100:0, 75:25, 50:50, 25:75 and 0:100 were studied for a depth insight into their interaction. FTIR analyses were also done to investigate the interaction between the XG and LPSG.

Results FTIR results indicated the hydrogen bond formation between the hydrocolloids. At the linear viscoelastic region (LVE), XG-rich blends exhibited higher $\tan \delta_{LVE}$ and τ_y , but lower τ_f . The values of apparent viscosity (η_a) and complex viscosity (η^*) diminished with increasing shear rate/frequency, and XG and LPSG individual dispersions showed the greatest and the lowest values, respectively. Based on the extended Cox-Merz rule, a greater shift factor (a) is observed as the ratio of LPSG in the mixed gel increases. At higher fraction of LPSG, except for the fraction of 75%, the thixotropic behaviour appears to be less pronounced. The recovery parameter (R , %) obtained from in-shear structural recovery test decreased with increase in LPSG fraction. The results of non-isothermal kinetic analysis revealed higher thermodynamic incompatibility and immiscibility of LPSG-XG system in the presence of 75% XG. Moreover, according to the results of Cole-Cole plot, the greatest compatibility of LPSG and XG blends was for LPSG75-XG25 sample ($\beta = 0.87$), whereas the worst miscibility was found to be for LPSG25-XG75 one ($\beta = 1.02$).

Conclusions Different rheological properties could be obtained by blending various ratios of LPSG and XG, which in some ratios synergistic behaviour was observed. The wide variety of rheological properties obtained may be appropriate for the use of LPSG-XG mixtures in food industries and pharmaceutical and biomedical applications.

Keywords *Lepidium perfoliatum* seed gum, Xanthan gum, Rheology, Interaction, Synergy, Incompatibility

*Correspondence:

Alireza Yousefi

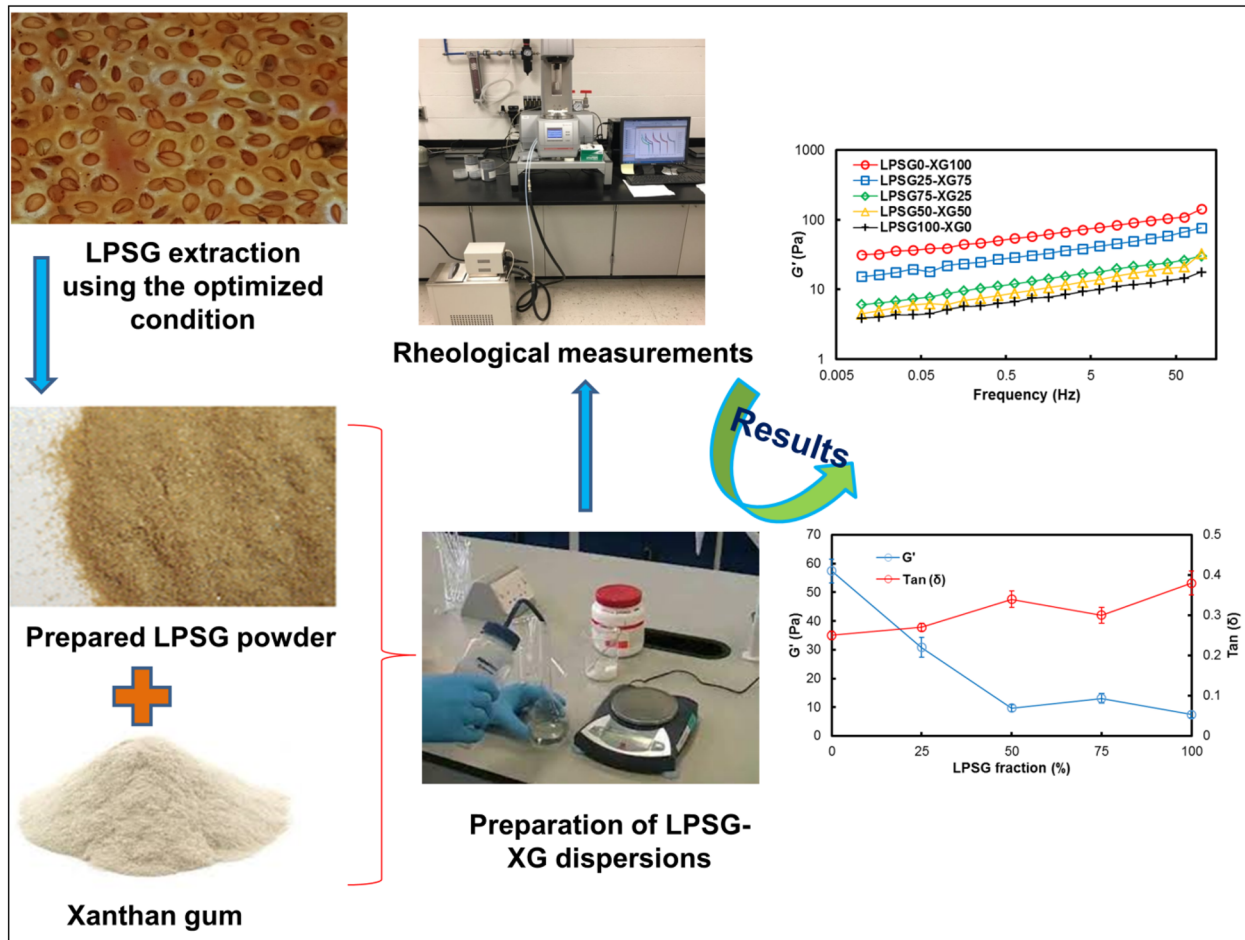
a_yousefi@ubonab.ac.ir; alireza.yousefi@univ-grenoble-alpes.fr

Full list of author information is available at the end of the article



© The Author(s) 2023. **Open Access** This article is licensed under a Creative Commons Attribution 4.0 International License, which permits use, sharing, adaptation, distribution and reproduction in any medium or format, as long as you give appropriate credit to the original author(s) and the source, provide a link to the Creative Commons licence, and indicate if changes were made. The images or other third party material in this article are included in the article's Creative Commons licence, unless indicated otherwise in a credit line to the material. If material is not included in the article's Creative Commons licence and your intended use is not permitted by statutory regulation or exceeds the permitted use, you will need to obtain permission directly from the copyright holder. To view a copy of this licence, visit <http://creativecommons.org/licenses/by/4.0/>. The Creative Commons Public Domain Dedication waiver (<http://creativecommons.org/publicdomain/zero/1.0/>) applies to the data made available in this article, unless otherwise stated in a credit line to the data.

Graphical Abstract



Introduction

The application of polysaccharides in formulation industries is growing due to their functional attributes, such as thickening, gelling, emulsifying abilities, etc. *Lepidium perfoliatum* is native to Europe and Asia, and the mucilage removed from its seed has been consumed owing to the pharmaceutical influences [1]. Recently, it has been reported that this mucilage, *Lepidium perfoliatum* seed gum (LPSG), has potential to be used as a thickening and stabilizing agent in food/pharmaceutical systems due to the pseudoplastic behaviour of its dispersions [2, 3]. The optimized conditions to extract the mucilage was found to be at temperature of 48.1 °C, pH of 8, water to seed ratio of 30:1 and process time of 1.5 h [4]. It has been reported that xylose (14.27%), galacturonic acid (10.70%), arabinose (9.07%) and galactose (8.80%) are the main monosaccharide components of LPSG. LPSG has 14.83% uronic acid and the average molecular weight of this biopolymer is 2.34×10^5 g/mol [5]. A shear-thinning

behaviour of LPSG dispersions has been identified at various temperatures (5–65 °C) and concentrations (0.5–2%, w/w) [6]. LPSG dispersions (1.5–3%, w/v) have also been exhibited viscoelastic properties in the linear viscoelastic region (LVE) at the temperature range of 5–85 °C [7].

Xanthan (XG) gum is one of the commercial polysaccharide which has widely been used in food systems for a number of important reasons comprising emulsion stabilization, temperature stability, compatibility with food ingredients and its pseudoplastic rheological properties [8, 9]. This gum is known as a galactomannan type microbial polysaccharide with anionic nature which it is produced by fermentation from *Xanthomonas campestris*. The main chain of galactomannan is composed of a 1–4 linked β -(D)-mannose backbone which may be substituted by a α -(D)-galactose side units at the O(6) position [10]. XG solutions are shear thinning and their viscosity in addition to shear depends on temperature (both dissolution and measurement temperatures), the gum

concentration, concentration of salts and pH of solution [9, 11]. This pronounced shear-thinning behaviour is due to unique rigid, rod-like conformation of XG, which is more responsive to shear than a random coil conformation [12]. Moreover, XG solutions produce yield stress, which has been obtained by direct or indirect methods, even at low concentrations [13, 14]. At higher concentration and lower temperature the XG solutions exhibit gel-like behaviour, in which storage modulus (G') is higher than loss modulus (G'') and both are weakly dependent on the oscillation frequency in the accessible range [15, 16].

Study on physicochemical and rheological characterizations of gels obtained from mixed polysaccharides has been an intertwining field of research recently. Such studies continue to be improved for controlling and describing the mechanism of interaction and the attributes of blended gels. Several studies have focused on the interaction of XG with other polysaccharides including guar gum [17], konjac glucomannan [18–20], locust bean gum [10, 21], starch [13, 22, 23], sodium alginate [24, 25], sage seed gum [26], cress seed gum [27], etc. One of the hypotheses concerning the mechanism of gelation between XG and other polysaccharides is that the unsubstituted regions of the monosaccharide backbone attach to the surface of the XG helix, i.e. interaction takes place when XG has its ordered conformation [28, 29]. In a different approach, the reason has been mentioned to be the possibility of interaction between the side chains of XG and unsubstituted segments of the backbone of the polysaccharide [19, 30].

Potential functionalities as well as structure of polysaccharide gums in a wide range of application can be identified by the rheological assessments. Different rheological techniques could be used in order to quantitatively characterize the interchain associations in gum mixture. Despite the progressive studies on physical and chemical properties of LPSG, it seems necessary to get more comprehensive understanding of the physical properties and structure of such emerging hydrocolloids, individually and in combination with other hydrocolloids, to meet the global needs for biopolymers for various applications. Finding the rheological synergistic interaction of LPSG and XG can help the use of LPSG as a novel food thickener in combination with XG, which in turn leads to consumption of lower concentrations of XG, which is relatively more expensive than LPSG, in food formulations. So, to have better idea in case of potential applications of LPSG, this research was taken to study the binary mixture of this emerging hydrocolloid with XG. For this reason, the impact of different ratios of the biopolymer mixtures (LPSG–XG%: 0–100, 25–75, 50–50, 75–25 and 100–0) on steady and oscillatory shear flow behaviour was studied.

A detailed information about the rheological characterization of the mixed gels were given using amplitude and frequency sweep experiments. A new approach was taken to extract thermodynamic parameters (ΔG° , ψ , ΔS , ΔH) based on temperature sweep test. Applicable rheological models were used to describe the rheological behaviour the mixtures in both steady and dynamic measurements. FTIR analysis was also carried out to investigate the chemical characteristics of the mixtures.

Materials and methods

Materials

Lepidium perfoliatum seeds were provided by a medical plant supplier in Tabriz, Iran. The seeds were then manually cleaned to remove all the impurities which visually could be identified. The *Lepidium perfoliatum* seed gum (LPSG) with average molecular weight of 2.34×10^5 Da was obtained according to the method described by Yousefi and Ako [2]. Xanthan gum with average molecular weight of 2×10^6 Da was purchased from Kelco (a division of Merck Co., New Jersey, USA).

Preparation of LPSG-XG mixtures

LPSG was mixed with XG with the proportions (% w/w) of 100-0 (LPSG100-XG0), 75-25 (LPSG75-XG25), 50-50 (LPSG50-XG50), 25-75 (LPSG25-XG75) and 0-100 (LPSG0-XG100), and the final concentration of all the mixtures was kept at 1% (w/w). For solution preparing, the mixture gum powders were dissolved in ultrapure water and stirred by a magnetic stirrer (25 °C, 400 rpm) for overnight in order to be sure that complete hydration will be taken place. Sodium azide (0.01% w/w) was added to the solutions to inhibit microbial contamination.

FTIR analysis

To obtain the FTIR spectra, the gel samples of LPSG, XG and LPSG-XG were lyophilized and pulverized under liquid nitrogen to provide fine powders. FTIR studies for each sample were done in triplicate using a spectrophotometer equipped with an UATR accessory (PerkinElmer, USA). Spectra were achieved over the range of 400 to 4000 cm^{-1} at 2 cm^{-1} of resolution.

Rheological characterizations

In this work, a DHR3 Controlled stress/strain rheometer (TA Instruments, New Castle, England) equipped with a parallel-plate probe (60 mm diameter and 500 μm gap) was exploited to carry out all the rheological measurements.

Oscillatory shear test

Strain sweep test

As the dynamic measurements were carried out in the linear viscoelastic region (LVE), the amplitude sweep experiments (0.1–250%) in controlled shear stress and controlled shear rate modes were implemented (25 °C, 1 Hz) to gain a strain corresponding to this region. It was found that for all gel samples a 0.50% strain was completely within the LVE range, and it was selected to perform all dynamic measurements.

Frequency sweep test

Frequency sweep experiment was done by subjecting the gels to oscillatory measurements at a frequency range of 0.01–100 Hz and a constant strain at LVE region (strain of 0.50%). TA Instruments Trios (version 4.0.1.29891) data analysis software was applied for determination of dynamic rheological parameters, including the storage modulus (G'), loss modulus (G''), loss tangent ($\tan \delta$) and complex viscosity (η^*) and analyse the rheological results at 25 °C.

It has been stated that the frequency dependency of G' and G'' values shows a power-law relation [Eqs. (1) and (2)] for a physical gel [31]:

$$G' = k' \times \omega^{n'}, \quad (1)$$

$$G'' = k'' \times \omega^{n''}, \quad (2)$$

where G' is the storage modulus, G'' is the loss modulus, ω is the oscillation frequency and k' and k'' are model constants. The constant n' and n'' are the slope in a log–log plot of G' and G'' versus ω .

The power-law equation [Eq. (3)] was also fitted on the obtained complex viscosity (η^*)-angular velocity (ω) curve in which the k^* (Pa.s ^{n^*}) and n^* (dimensionless) are, respectively, intercept and slope of the curve:

$$\eta^* = k^* \omega^{(n^*-1)} \quad (3)$$

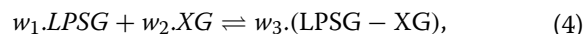
Temperature sweep test

A frequency of 0.1 Hz and a strain of 0.01% were applied to accomplish the temperature sweep test in the LVE region. The temperature of Peltier was set on 10 °C, and then sufficient amount of the samples was placed onto Peltier at this temperature and kept for 15 min. After applying the gap (500 μ m), the samples surpluses were carefully removed and the edges of the samples were covered with a thin film of silicon oil to prevent evaporation during the experiments. A temperature gradient sweep was performed within the range of 10–90 °C. For this purpose, the temperature was linearly increased and then decreased at the rate of 1 °C/min.

During the measurements, the values of complex modulus ($G^* = \sqrt{(G')^2 + (G'')^2}$) as a function of time and temperature were recorded.

Thermodynamic incompatibility

For this reason, the new method described by Razavi, Alghooneh [32]. Accordingly, the interaction of biopolymers as supposed to be a kind of equilibrium reaction as follows:



where w_1 is the weight fraction of LPSG, w_2 is the weight fraction of XG in the mixture and w_3 refers to the weight fraction of the LPSG-XG mixtures. Consequently, the equilibrium constant (K_{eq}) can be calculated [Eq. (5)] based on G^* parameter:

$$K_{eq} = \frac{(G^*_{LPSG-XG})^{w_3}}{(G^*_{LPSG})^{w_1} \times (G^*_{XG})^{w_2}} \quad (5)$$

In a reaction, supposed that the K_{eq} parameter can be connected to the standard Gibbs free energy change (ΔG°) as follows:

$$\Delta G^\circ = -RT \ln(K_{eq}) \quad (6)$$

Based on this equation, the value of $[-\ln(K_{eq})]$, the ψ parameter, can be used as a representative of ΔG° . Furthermore, the changes in enthalpy (ΔS , J/mol. $^\circ$ K) and entropy (ΔH , J/mol) of the supposed reactions over the temperature sweep experiments were obtained using Eqs. (7) and (8), [33], respectively:

$$\Delta S = R \times \ln \left(\frac{K_0 \times N_A \times h}{2.72RT} \right), \quad (7)$$

$$\Delta H = \Delta G + T \Delta S, \quad (8)$$

In which K_0 is the frequency factor (dimensionless), N_A is the Avogadro constant (mol⁻¹) and h is the Planck constant (J.s).

The frequency factor and activation energy (E_a) can be obtained based on a combination of the classic rate equation, Arrhenius equation and time–temperature relationship developed by Rhim, Nunes [34]. The following relation [Eq. (9)] is a general form of non-isothermal kinetic analysis based on complex modulus (G^*) attained from temperature sweep test, which is in connection with the structure development or degradation of materials:

$$\ln \left(\frac{1}{G^{*m}} \times \frac{dG^*}{dt} \right) = \ln k_0 + \left(\frac{E_a}{RT} \right), \quad (9)$$

In which m is the order of reaction, t is time (s), k_0 is the Arrhenius pre-exponential or frequency factor, E_a is the

activation energy (J/mol) and R and T are, respectively, the universal gas constant (J/mol K) and the absolute temperature (K).

Material stiffness parameter

Based on some assumptions expressed by Friedrich and Heymann [35] in case of calculating the viscoelastic modules in the LVE domain, at high frequency range or near the gel point, the following relation, Eq. (10), can be exploited to calculate the material stiffness parameter [36]:

$$G^* \cong \left(\frac{2}{\pi}\right)^{0.5} S_{\alpha}^* \omega^{\alpha} = A_{\alpha} \omega^{\alpha}, \quad (10)$$

where α is the order of relation function, S_{α}^* is a parameter dependent on the stiffness of materials and A_{α} is the material stiffness parameter ($\text{Pa}\cdot\text{rad}^{-\alpha}\cdot\text{s}^{\alpha}$).

Steady shear test

Steady shear measurements

In this case, shear stress (τ)–shear rate ($\dot{\gamma}$) data were obtained at strain-controlled mode by applying the shear rate in the range of 0.01–500 s^{-1} to the LPSG-XG mixtures at 25 °C. The power law (Ostwald-De Waele) [Eq. (11)] was used to describe the time-independent flow behaviour of the mixtures [37]:

$$\eta_a = k \dot{\gamma}^{(n-1)}, \quad (11)$$

In which k ($\text{Pa}\cdot\text{s}^n$) and n are the power-law consistency coefficient and flow behaviour index, respectively.

Thixotropy measurements

In order to determine the time dependency of the LPSG–XG mixtures, the shear rate was increased from 0.01 to 500 s^{-1} during 180 s and then decreased at the same time from 500 to 0.01 s^{-1} . The hysteresis loop was calculated from the area between the upstream and downstream stress–strain data. Then, the area was measured by the difference between integrating the area for forward and backward measurements from initial shear rate ($\dot{\gamma}_1$) to final shear rate ($\dot{\gamma}_2$) as follows [Eq. (12)]:

$$\text{Hysteresis loop area} = \int_{\dot{\gamma}_1}^{\dot{\gamma}_2} k_p \dot{\gamma}^{n_p} - \int_{\dot{\gamma}_1}^{\dot{\gamma}_2} k'_p \dot{\gamma}^{n'_p}, \quad (12)$$

where k_p , k'_p , n_p and n'_p are the consistency coefficient and flow behaviour index for forward and backward measurements, respectively.

Based on the method described by Mezger [38], in-shear structural recovery of the LPSG-XG samples was measured. Hence, three consecutive shear flows were implemented as follows: (a) after pre-shearing at 1 s^{-1} for 30 s, the samples subjected to shear rate of 1 s^{-1} for

2 min, (b) shear rate of 300 s^{-1} was applied for 1 min and eventually (c) the samples was again subjected to the shear rate of 1 s^{-1} for 2 min. Accordingly, the magnitude of recovery of the samples (R , %) was calculated as the percentage ratio of average η_a gained during the first 30 s of the third step to average η_a value recorded in the first step.

Moreover, for better understanding of the structural features of time-dependent behaviour of the mixtures, first-order stress decay model [Eq. (13)] was fitted on the shear stress (τ)–time (t) data obtained from the third step of the flow measurement [step (c)]:

$$\tau - \tau_{eq} = (\tau_0 - \tau_{eq}) e^{-kt}, \quad (13)$$

where τ_0 implies the immediate recovered structure, and τ_{eq} (Pa) indicates the structural stability of recovered material, and k (s^{-1}) exhibits the rate of recovery.

Yield stress measurements

The yield stress values of LPSG-XG mixtures were directly calculated by linearly ramping of stress from 0.1 to 20 Pa over 120 s. Afterwards, the obtained apparent viscosities were plotted against the applied stresses. Results show an increment in the viscosity as long as the structure is maintained (elastic behaviour), followed by a sharp decrement in the viscosity as the structure collapses and the material starts to flow (fluid behaviour). The stress corresponding to the maximum apparent viscosity is considered as the yield stress (Steffe, [37]).

Interaction coefficient measurements

The following equation described by Razi, Motamed-zadegan [39] was used to find out the synergistic or antagonistic influence of the incorporations of the gums in the mixtures compared to the weight averages of the single component systems for all the rheological parameters studied:

$$\alpha(\%) = \frac{\text{Exp} \cdot (\text{LPSG-XG}) - (w_1 \times \text{Exp} \cdot \text{LPSG} + w_2 \times \text{Exp} \cdot \text{XG})}{\text{Exp} \cdot (\text{LPSG-XG})}, \quad (14)$$

where $\text{Exp} \cdot (\text{LPSG-XG})$, $\text{Exp} \cdot \text{LPSG}$ and $\text{Exp} \cdot \text{XG}$ are the parameters obtained from the rheological experiments for LPSG–XG mixtures, LPSG and XG, respectively.

Results and discussions

FTIR characterization

To further study the interaction between the XG and LPSG, any changes in the position and intensity of the vibration bands were analysed by FTIR analysis. FTIR spectra of the lyophilized LPSG-XG samples are shown in Fig. 1. In the FTIR spectrum of XG, the stretching

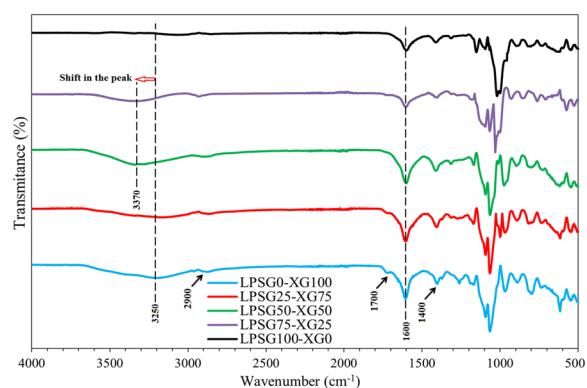


Fig. 1 Impact of various ratios of LPSG on FTIR spectra of LPSG-XG blends; LPSG *Lepidium perfoliatum* seed gum; XG xanthan gum

vibration of $-O-H$ bond (and hydrogen bond) is seen as a typical broad band at about 3250 cm^{-1} . The peaks at about 2900 cm^{-1} are attributed to the symmetric and asymmetric stretching vibration of the SP^3-C-H bonds. The two characteristic peaks at about 1700 and 1600 cm^{-1} can be assigned to the stretching modes of $-C=O$ (carbonyl) bonds of the ester and ether groups. The peaks related to the symmetric and asymmetric bending vibration modes of $-C-H$ bonds are observed at about 1400 cm^{-1} . The peaks appearing at $1000-1250\text{ cm}^{-1}$ are related to the stretching vibration of $-C-O$ bonds [40, 41]. The out-of-plane bending vibration modes of $-O-H$ bonds are appeared at about 950 cm^{-1} . The LPSG FTIR spectrum has different peaks compared to the XG spectrum, and the very weak peak of $-O-H$ bond at 3250 cm^{-1} indicated lower $-O-H$ content of LPSG [42]. All the composite samples of LPSG and XG have weaker the $-O-H$ bond peak, indicating the hydrogen bond formation between the LPSG and XG, particularly for the LPSG75-XG25 sample, which was accompanied with the shift in the $-O-H$ peak from 3250 to 3370 cm^{-1} . Additionally, enhancement of the intensity of the bands at about 1600 cm^{-1} indicates the interaction between XG and LPSG [43].

Oscillatory strain

In the linear viscoelastic region (LVE), the extent of elastic (G') and viscos (G'') modulus is roughly constant, while in the non-linear region both start to diminish (Fig. 2). The strain at which the value of G' is sharply decreased due to the deformability of the LPSG-XG mixtures. The rheological parameters at LVE including loss tangent ($\tan \delta_{LVE}$), yield stress (τ_y) and flow-point stress (τ_f) with corresponding modulus (G_f ; $G' = G''$) were determined and are represented in Table 1. The values of $\tan \delta_{LVE}$, which indicates the physical behaviour of gel

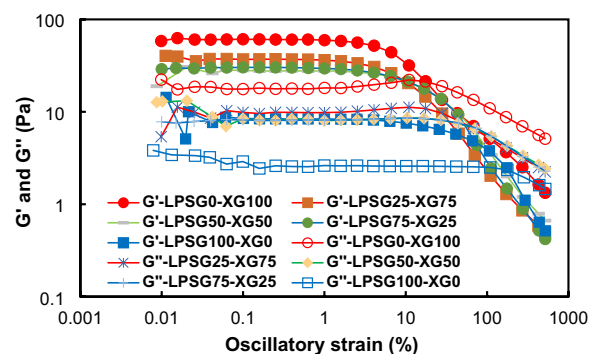


Fig. 2 Strain sweep dependence of storage modulus (G') and loss modulus (G'') for LPSG and XG blends (1 Hz, $25\text{ }^\circ\text{C}$); LPSG *Lepidium perfoliatum* seed gum; XG xanthan gum

systems, were within the range of $0.281-0.312$, indicating a predominantly elastic behaviour of the samples at the LVE region. No significant difference was found between the $\tan \delta_{LVE}$ values of LPSG50-XG50 and LPSG75-XG25 ($p > 0.05$) samples, while for the others, lower values were obtained at higher ratios of XG. As it can be seen, the samples with higher extent of XG (LPSG0-XG100 and LPSG25-XG75) exhibited significantly ($p < 0.05$) greater yield stress (τ_y) values ($0.37-62\text{ Pa}$). In other words, it can be stated that resistance to the stress applied to these gels, which indicates the starting point of weakening of the gel strength, was more than the other gels [44]. Out of the LVE region where the G' cross G'' (flow point), the structure is ruptured and the system starts to flow. In the contrast to the aforementioned results, the corresponding stress for this point (τ_f), which implies the yield stress at the flow point, was found to be greater for the systems containing higher levels of LPSG. Large values of τ_f for LPSG dispersions at the LVE region has previously been reported at different concentrations ($1.5-3\%$) and temperatures ($5-85\text{ }^\circ\text{C}$) [7].

Steady shear- and frequency-dependent behaviour

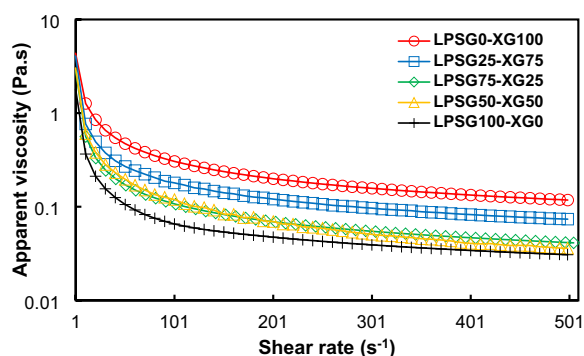
The shear-dependent viscosity curve obtained for individual gum samples and their blends are represented in Fig. 3. As shear rate was raised up to 500 s^{-1} , the apparent viscosity of all samples decreased, indicating their shear-thinning behaviour. As it is evident, the samples containing higher ratios of XG noticeably represented greater values of apparent viscosity, except in the case of LPSG50-XG50 and LPSG75-XG25, in which no significant difference was observed ($p > 0.05$). The power-law equation [Eq. (11)] fitted well ($R^2 \geq 0.98$) on the experimental data and its parameters are shown in Table 2. As the ratio of LPSG in the gum mixtures was enhanced from 0 to 100%, the consistency coefficient (k) was reduced up to 72%. In the case of flow behaviour index

Table 1 The rheological parameters obtained from the linear viscoelastic region (LVR) for different ratios of LPSG-XG blends (1 Hz, 25 °C)^{a,b}

Parameters	LPSG-XG (%)				
	LPSG0-XG100	LPSG25-XG75	LPSG50-XG50	LPSG75-XG25	LPSG100-XG0
$\tan(\delta_{LVE})$	0.28 ± 0.00 ^C	0.28 ± 0.00 ^C	0.30 ± 0.00 ^B	0.29 ± 0.00 ^B	0.31 ± 0.00 ^A
τ_y (Pa)	0.62 ± 0.09 ^A	0.37 ± 0.06 ^B	0.25 ± 0.03 ^C	0.21 ± 0.03 ^C	0.22 ± 0.04 ^C
τ_f (Pa)	5.26 ± 0.25 ^B	3.81 ± 0.17 ^C	6.12 ± 0.40 ^A	5.91 ± 0.22 ^A	5.98 ± 0.36 ^A

^a Values in rows with different letters are significantly different ($P \leq 0.05$)

^b LPSG *Lepidium perfoliatum* seed gum, XG xanthan gum

**Fig. 3** Time-independent flow curves for different ratios of LPSG-XG blends; LPSG *Lepidium perfoliatum* seed gum; XG xanthan gum

(n), no significant difference ($p > 0.05$) was detected between the mixtures containing 0%, 25% and 100% LPSG, while LPSG50-XG50 and LPSG75-XG25 samples revealed significantly lower values (more pseudoplasticity) ($p < 0.05$). The pseudoplasticity of hydrocolloids allows liquid foods to be pumped easily and it is also aligned with a lower degree of sliminess in the mouth during swallowing [45, 46].

The variation of G' and G'' with frequency for the gel samples is given in Fig. 4a, b. As it is evident from the magnitude of the moduli, the G' values of all the samples

were constantly over the G'' ones with low frequency dependence, which implies solid-like behaviour. The fitting results indicated the appropriateness of power-law equations [Eqs. (1) and (2)] for describing the frequency dependence of the moduli ($R^2 \geq 0.86$) (Table 3). From the results, a low frequency dependency of G' ($0.15 \leq n' \leq 0.19$) and G'' ($0.15 \leq n'' \leq 0.25$) was detected for all the samples, which reflected the characteristics of weak gel. This characteristic was also confirmed from the ratio of G'/G'' ($2.46 \leq k'/k'' \leq 3.63$), which were lower than 10 folds [37]. Weak physical gels have reversible links, i.e. hydrogen bonds or ionic associations, formed from temporary associations between polymer chains. These associations have finite lifetime, breaking and reforming continuously [47]. The k' and k'' parameters drastically diminished, respectively, 87% and 436%, as the LPSG fraction in the mixtures was increased, while in the case of n' and n'' there were not significant differences between most of the samples ($p > 0.05$).

The frequency dependence of complex viscosity (η^*) over the frequency range of 0.01–100 Hz was assessed and the results are depicted in Fig. 4c. The values of η^* diminished with increasing frequency, and XG and LPSG individual dispersions showed the greatest and the lowest η^* values, respectively. This decrement in value of η^* is due to the further destruction of structure at higher

Table 2 The power-law parameters obtained from the steady shear and oscillatory shear tests of the different ratios of LPSG-XG blends^{a,b}

LPSG-XG (%)	$\eta_a = k\dot{\gamma}^{(n-1)}$			$\eta^* = k^*\omega^{(n^*-1)}$		
	k (Pa.s ⁿ)	n	R^2	k^* (Pa.s ⁿ)	n^*	R^2
LPSG0-XG100	4.67 ± 0.11 ^a	0.41 ± 0.02 ^a	0.99	8.63 ± 0.18 ^a	0.11 ± 0.00 ^c	0.99
LPSG25-XG75	3.18 ± 0.14 ^b	0.39 ± 0.01 ^a	0.98	4.89 ± 0.14 ^b	0.14 ± 0.00 ^b	0.99
LPSG50-XG50	2.98 ± 0.09 ^c	0.33 ± 0.01 ^b	0.99	1.39 ± 0.07 ^d	0.15 ± 0.01 ^b	0.99
LPSG75-XG25	2.38 ± 0.13 ^d	0.34 ± 0.02 ^b	0.99	2.10 ± 0.10 ^c	0.17 ± 0.01 ^a	0.99
LPSG100-XG0	1.30 ± 0.10 ^e	0.38 ± 0.03 ^a	0.98	0.79 ± 0.04 ^e	0.10 ± 0.00 ^c	0.99

^a Values in columns with different letters are significantly different ($P \leq 0.05$)

^b LPSG *Lepidium perfoliatum* seed gum, XG xanthan gum

Table 3 Power-law parameters of storage modulus (G'), loss modulus (G'') and complex modulus (G^*) for the different ratios of LPSG-XG blends (0.50% strain, 25 °C)^{a,b}

LPSG-XG (%)	$G' = k' \times \omega^{n'}$			$G'' = k'' \times \omega^{n''}$			$G^* = A_\alpha \omega^\alpha$		
	k' (Pa.s ^{n'})	n'	R^2	k'' (Pa.s ^{n''})	n''	R^2	A_α	α	R^2
LPSG0-XG100	59.50 ± 3.74 ^a	0.15 ± 0.01 ^b	0.99	16.36	0.15 ± 0.00 ^c	0.97	46.46	0.14	0.99
LPSG25-XG75	31.72 ± 1.33 ^b	0.17 ± 0.00 ^b	0.99	9.35	0.23 ± 0.01 ^b	0.96	24.09	0.16	0.99
LPSG50-XG50	10.18 ± 0.60 ^d	0.19 ± 0.02 ^{ab}	0.98	3.58	0.22 ± 0.01 ^b	0.92	7.56	0.17	0.99
LPSG75-XG25	13.07 ± 0.56 ^c	0.17 ± 0.00 ^{ab}	0.99	4.93	0.25 ± 0.01 ^a	0.87	9.99	0.17	0.99
LPSG100-XG0	7.49 ± 0.81 ^e	0.16 ± 0.00 ^b	0.99	3.05	0.25 ± 0.01 ^a	0.86	5.88	0.16	0.99

^a Values in columns with different letters are significantly different ($P \leq 0.05$)

^b LPSG *Lepidium perfoliatum* seed gum, XG xanthan gum

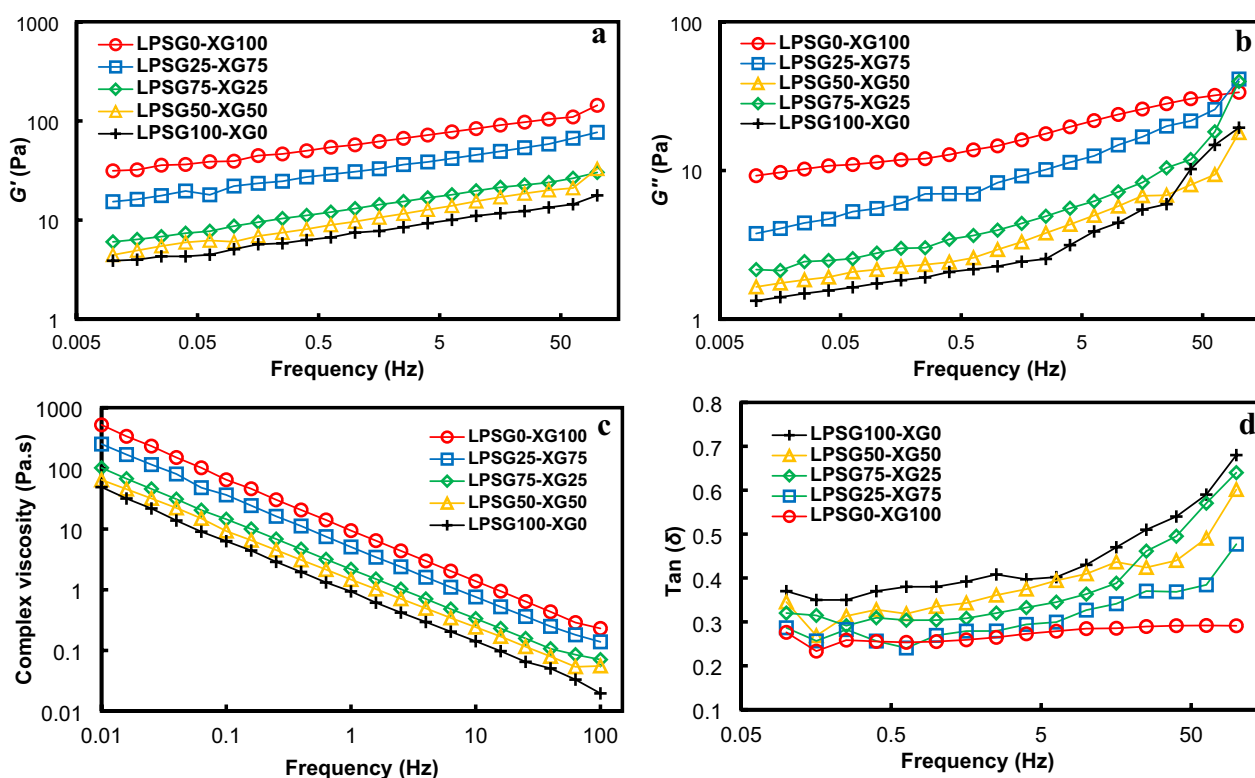


Fig. 4 Frequency dependence of **a** storage modulus (G'); **b** loss modulus (G''); **c** complex viscosity (η^*); and **d** loss tangent ($\tan \delta$) for different ratios of LPSG-XG blends (0.50% strain, 25 °C); LPSG *Lepidium perfoliatum* seed gum, XG xanthan gum

frequency and indicates the pseudoplasticity under small deformation. The absolute values of the slopes obtained from complex viscosity–frequency curves were within the range 0.80–0.85 (data not shown), which were higher than the critical value of 0.76, representing a weak gel polysaccharide formed by overlapping and entanglements of flexible random coil chains [48]. Similar results have been reported for xanthan gum-creess seed gum [27] and sage seed gum-xanthan gum blends [26].

Based on the results of loss tangent ($\tan \delta$) shown in Fig. 4d, this characteristic was almost frequency

independent entire the frequency range applied for XG. In comparison, the other samples showed various degrees of dependency for the frequencies >2.5 Hz (LPSG25-XG75), >1.58 Hz (LPSG75-XG25), >0.40 Hz (LPSG50-XG50) and >0.25 Hz (LPSG100-XG0). Loss tangent is considered as one of the most common dynamic rheological parameters employed for description of viscoelastic behaviour, and the values of $\tan \delta < 1$ and $\tan \delta > 1$ are dedicated to the concepts of predominantly elastic and viscous behaviours, respectively [44, 49]. The magnitudes of $\tan \delta$ for all the samples found to be in

the range of 0.16–0.68, which indicates an intermediate behaviour between a weak and a strong elastic gel.

The results of dynamic tests obviously revealed that increase in LPSG fraction in the LPSG-XG mixtures almost resulted in a lower value of complex viscosity and elastic moduli, but a higher value of $\tan \delta$ (Fig. 5a, b). All these results confirm the existence of a stronger gel structure at a higher fraction of XG. As can be observed, the only exception among the samples was LPSG75-XG25, which indicated the characteristics of a stronger structure compared to LPSG50-XG50. This variation in rheological properties resulting from the difference in mixing ratios of hydrocolloids has already been reported for xanthan gum-glucomannans [28], xanthan gum-locust bean gum [10, 50], sage seed gum-xanthan gum [26], vinal gum-xanthan gum [51] and xanthan gum-cress seed gum [27].

Applicability of the Cox-Merz rule

The *Cox-Merz* rule has been proposed by Cox and Merz [52], and this rule involves steady shear viscosity (η_a) and complex viscosity (η^*) measured at a small oscillatory strain, as follows (Eq. (15)):

$$\eta_a(\dot{\gamma}) = |\eta^*(\omega)|_{\omega=\dot{\gamma}} \quad (15)$$

It is applicable for vary of polymer solutions, especially when the measurement of viscosity at higher shear rate

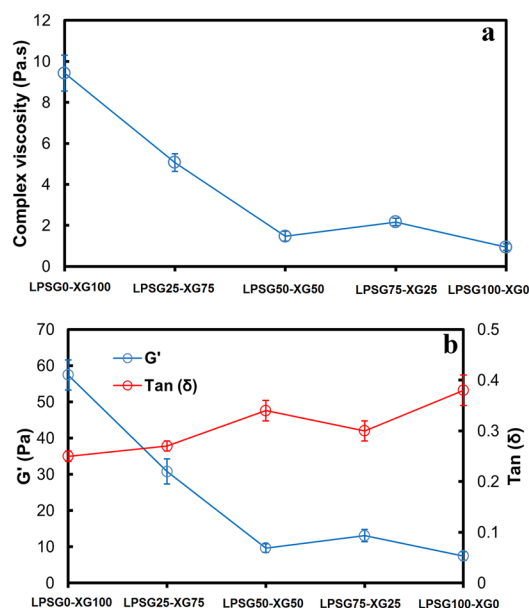


Fig. 5 Influence of various ratios of LPSG on **a** complex viscosity (η^*); and **b** storage modulus (G') and loss tangent ($\tan \delta$) of LPSG-XG blends (1 Hz, 25 °C); LPSG *Lepidium perfoliatum* seed gum, XG xanthan gum

region from the oscillatory strain measurements is difficult because of the sample fracture, secondary flow, etc. [53]. By entering α parameter which is the shift factor, this equation is changed as Eq. (16) and it is called the extended or modified *Cox-Merz* rule:

$$\eta_a(\dot{\gamma}) = |\eta^*(\alpha.\omega)|_{\omega=\dot{\gamma}} \quad (16)$$

The extent of departure from *Cox-Merz* rule (β) can be obtained from the areas calculated by the flowing integral equation (Eq. (17)):

$$\beta = \frac{\text{abs}\left(\int_{\omega_0}^{\omega} \eta^* d\omega - \int_{\dot{\gamma}_0}^{\dot{\gamma}} \eta_a d\dot{\gamma}\right)}{\int_{\omega_0}^{\omega} \eta^* d\omega} \quad (17)$$

The results, obtained at the frequency range of 0.1–100 Hz and the shear rate range of 0.1–100 s^{-1} , revealed that as the ratio of LPSG in the mixed gel increases, more shift is observed and the value of α parameter raises from 0.69 to 3.67 (Table 4). The values of α parameter greater than unity attained for almost all the samples, except XG, imply that the complex viscosity ($|\eta^*(\omega)|$) is almost always smaller than the steady shear viscosity ($\eta_a(\dot{\gamma})$) at the given range of frequency/shear rate. This behaviour is not very relevant for biopolymeric solutions, but it has been found in some studies for semidilute solutions of xanthan gum in 0.5% NaCl [54], aqueous solutions of hydroxyethyl guar gum [55], several concentrations of high-methoxyl pectin [56] and high concentrations of vinal gum solutions [51]. Although the *Cox-Merz* superposition rule has apparently been confirmed for some hydrocolloid solutions [56–58], but this rule has been not obeyed by biopolymeric dispersions without applying the shift factor. The same behaviour in case of β values was also observed for all the samples, except LPSG75-XG25, influenced by the increment in the level of LPSG in the blends (Table 4). The greatest and the lowest values of β were found for LPSG (2.85) and XG (0.35) individual

Table 4 The extended *Cox-Merz* model constant (α) and the extent of departure parameter (β) for the different ratios of LPSG-XG blends^a

LPSG-XG (%)	$\eta(\dot{\gamma}) = \eta^*(\alpha.\omega) _{\omega=\dot{\gamma}}$		β
	α	R^2	
LPSG0-XG100	0.69	0.98	0.35
LPSG25-XG75	1.01	0.96	0.40
LPSG50-XG50	1.74	0.99	2.69
LPSG75-XG25	2.85	0.99	0.91
LPSG100-XG0	3.67	0.97	2.85

^a LPSG *Lepidium perfoliatum* seed gum, XG xanthan gum

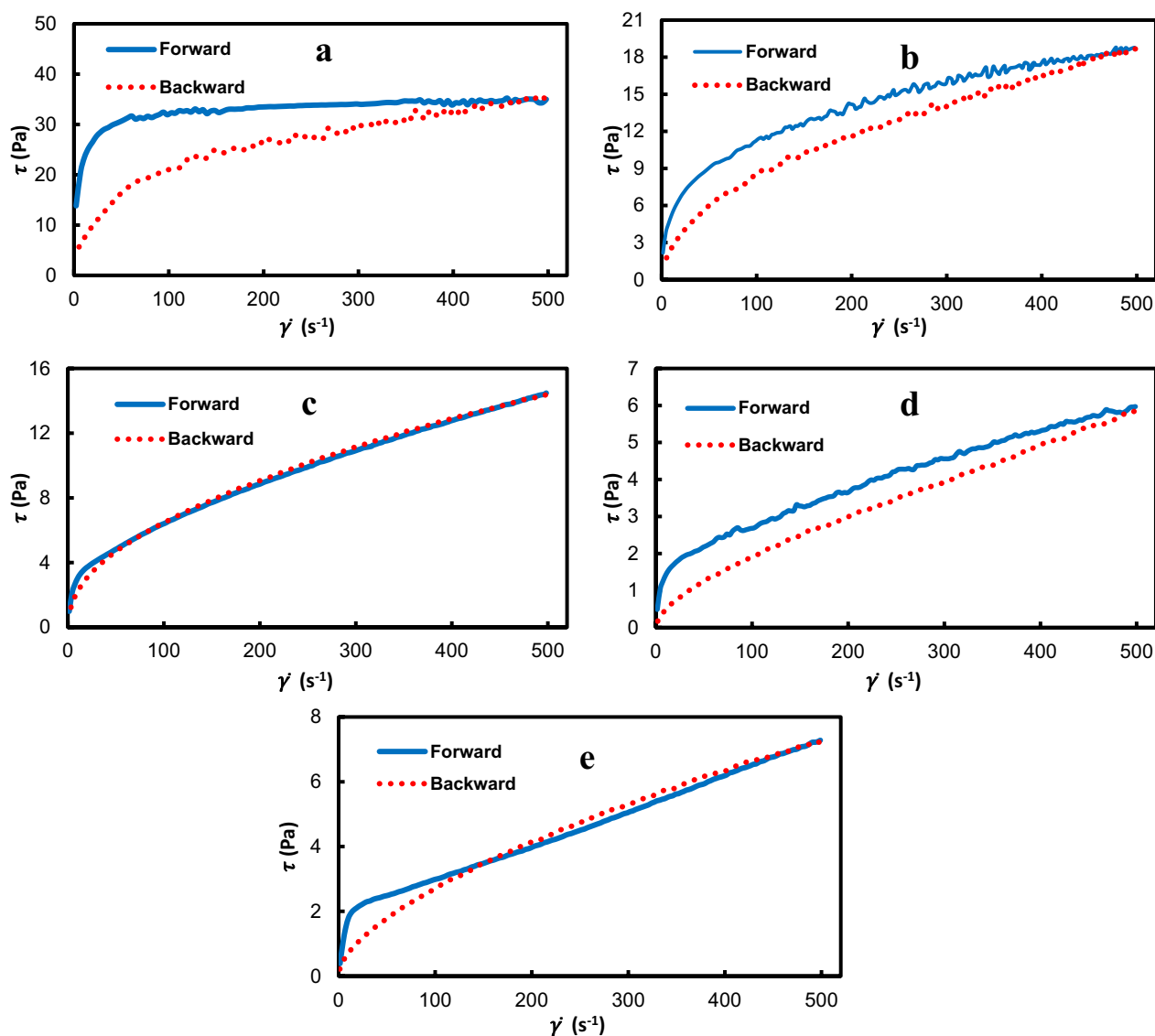


Fig. 6 The shear loop test curves obtained for different ratios of LPSG-XG blends **a** LPSG0-XG100, **b** LPSG25-XG75, **c** LPSG50-XG50, **d** LPSG75-XG25, **e** LPSG100-XG0; LPSG *Lepidium perfoliatum* seed gum, XG xanthan gum

gels, respectively. This departure for polymeric dispersions may be associated with either the presence of hyper-entanglements, i.e. high density entanglements, or aggregates [59, 60]. It has been suggested that departure from the *Cox-Merz* rule is related to the characteristics of a weak gel structure for sage seed gum-xanthan blends [26]. It is likely that a similar mechanism is happening in our systems, LPSG gel has a weaker gel structure, which is in agreement with the results of Table 1, where a greater value of $\tan(\delta_{LVE})$ (0.312) has been reported for this sample.

Thixotropic behaviour

The results attained from shear loop test of the LPSG-XG blends are depicted in Fig. 6. As shown in Table 5, the maximum (20.86%) and the minimum (0.88%) amount of hysteresis loop area were observed for XG and LPSG individual gum samples, respectively. It means that the rate of macromolecules disentanglement induced by shear for XG was higher than their re-entanglement compared to the others. Comparatively, these results indicate the sensitivity of LPSG to shear history and its weaker thixotropic behaviour. From the results, thixotropy appears to be less pronounced at higher fraction of LPSG, but at fraction of 75% LPSG, an increase in

Table 5 The parameters of power-law model and the hysteresis loop area values obtained from shear loop test of the different ratios of LPSG-XG blends^{a,b}

LPSG-XG (%)	Forward			Backward			Hysteresis loop area (%)
	k_p (Pa.s ⁿ)	n_p	R^2	k'_p (Pa.s ⁿ)	n'_p	R^2	
LPSG0-XG100	22.54 ± 1.86 ^a	0.08 ± 0.01 ^c	0.91	3.51 ± 0.22 ^a	0.38 ± 0.02 ^c	0.98	20.86
LPSG25-XG75	2.40 ± 0.08 ^b	0.33 ± 0.07 ^b	0.99	0.81 ± 0.04 ^b	0.50 ± 0.05 ^b	0.99	13.74
LPSG50-XG50	0.91 ± 0.05 ^c	0.44 ± 0.03 ^a	0.99	0.70 ± 0.06 ^c	0.48 ± 0.03 ^b	0.99	4.29
LPSG75-XG25	0.47 ± 0.02 ^d	0.40 ± 0.06 ^a	0.98	0.10 ± 0.02 ^e	0.64 ± 0.03 ^a	0.99	19.35
LPSG100-XG0	0.49 ± 0.04 ^d	0.41 ± 0.04 ^a	0.95	0.17 ± 0.03 ^d	0.60 ± 0.05 ^a	0.99	0.88

^a Values in columns with different letters are significantly different ($P \leq 0.05$)

^b LPSG *Lepidium perfoliatum* seed gum, XG xanthan gum

Table 6 The first-order stress decay model parameters and the recovery parameter (R , %) obtained for the different ratios of LPSG-XG blends^{a,b}

LPSG-XG (%)	τ_0 (Pa)	τ_{eq} (Pa)	k (s ⁻¹)	R^2	R (%)
LPSG0-XG100	4.34 ± 0.16 ^a	4.53 ± 0.09 ^a	0.099 ± 0.013 ^a	0.96	80.52
LPSG25-XG75	2.09 ± 0.10 ^b	2.19 ± 0.06 ^c	0.032 ± 0.008 ^c	0.93	68.54
LPSG50-XG50	1.88 ± 0.05 ^c	2.73 ± 0.11 ^b	0.029 ± 0.003 ^c	0.99	53.42
LPSG75-XG25	1.78 ± 0.07 ^c	2.12 ± 0.04 ^c	0.044 ± 0.009 ^b	0.96	42.91
LPSG100-XG0	1.07 ± 0.04 ^d	1.59 ± 0.04 ^d	0.035 ± 0.006 ^{bc}	0.95	34.43

^a Values in columns with different letters are significantly different ($P \leq 0.05$)

^b LPSG *Lepidium perfoliatum* seed gum, XG xanthan gum

thixotropy behaviour was observed which showed no significant difference with that of XG ($p > 0.05$). According to the results presented in Table 5, the power-law consistency coefficient ($k_p = 0.47$ – 22.54) and flow behaviour index ($n_p = 0.08$ – 0.44) for forward curves were higher and lower than those of backward curves ($k'_p = 0.10$ – 3.51 , $n'_p = 0.38$ – 0.64), respectively. Consequently, it can be supposed that the structure of the samples has, to some extent, been destroyed during applying shear rate in forward state. Almost for all the samples, increase in LPSG fraction resulted in a decrease in k_p and k'_p parameters and an increase in n_p and n'_p ones, respectively.

According to the results of in-shear structural recovery test (Table 6), the recovery parameter (R , %), which considers as an indicator of the recovered structure, decreased from 80.52 to 34.43% with increase in LPSG fraction from 0 to 100%. This parameter is concerned with the recovered structure after high shear degradation and is associated to particle rearrangements or microstructure rebuilding at rest [26, 61]. In order to provide a detailed information about the mechanism of structure recovery, the first-order stress decay model (Eq. (13)) was used for description of the single influence of time, which could appropriately fitted on the experimental data ($R^2 > 0.93$). The results obtained for the immediate

recovered structure parameter (τ_0), which reflects the extent of elastic component materials in high deformation, revealed that XG and LPSG had, respectively, the highest (4.34 Pa) and the lowest (1.07 Pa) values. The same trend was also observed in the case of the stress value at equilibrium plateau (τ_{eq}) with value of 4.53 Pa for XG, and value of 1.59 Pa for LPSG. This result indicates XG has a greater reforming of the agglomerates, which results in a stronger structure. The highest rate of recovery (k) was found for XG (0.099 s^{-1}), while there was not any significant difference between most of the samples. This parameter implies at which rate the material will be reached to its recovered plateau state when the stress totally or partially is removed.

Yield stress

Stress ramp technique, which is considered as the most frequently one among several methods used for determination of the yield stress of food systems [62, 63], was applied in this study. The yield stress results of the mentioned technique, which is called the static yield stress [64], are represented in Fig. 7. In this method, it is assumed that there is a critical stress, which is called yield stress, below which the material has elastic-like behaviour, and above which the structure collapses and start to flow. It means that before the yield stress the system is fully elastic and is still able to absorb the stress energy without altering its internal microstructure. Exactly after this point, the viscosity abruptly decreases, because the microstructure is changing and the system is unable to absorb more energy without being deformed [65]. With the increasing fraction of LPSG in the mixed system up to 50%, the magnitude of static yield stress constantly decreased (up to 33%). This yield stress value for LPSG75-XG25 was greater than that of LPSG50-XG50, and both LPSG50-XG50 and LPSG100-XG0 samples showed the lowest values. In addition to stress ramp method, the dynamic yield stress values were also precisely estimated

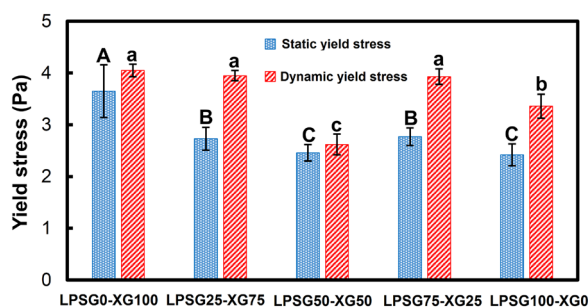


Fig. 7 The magnitude of static and dynamic yield stress values obtained for different ratios of LPSG-XG blends; Different letters on columns in each series indicate significant difference ($P \leq 0.05$); LPSG *Lepidium perfoliatum* seed gum, XG xanthan gum

by extrapolating stress value to the zero shear rate using the Herschel-Bulkley model ($R^2 = 0.995-0.999$, $RMSE = 0.145-0.366$) [66]. As represent in Fig. 7, there were not any significant difference between the dynamic yield stress values (3.92 Pa–4.05 Pa) of the samples containing 0%, 25% and 75% LPSG ($p > 0.05$) and they had the greatest values, whereas the lowest value was obtained for LPSG50-XG50 sample (2.62 Pa). The high yield stress of XG may come from interaction between its macromolecules and intermolecular association of acetate residues, where stable configuration can exhibit a resistant to flow [67, 68]. As it is evident, the dynamic yield stress values for all the samples were greater than those of the static yield stress (7–45%), which was in agreement with some results have been reported for the hydrocolloids mixtures [26, 69]. These results obviously demonstrated that all the gel samples had to some extent coherent network structures; therefore, they require to be subjected to a certain amount of stress to start the flow.

Activation energy and thermodynamic attributes

The estimated values of E_a based on the Eq. (9) showed that at the heating stage, as the ratio of SSG increases from 25 to 75%, the E_a values increases from 9.77 to 16.32 (kJ/mol) (Table 7). At this stage, SSG showed a pronounced higher value E_a than XG, indicating higher sensitivity of SSG network to temperature than that of XG. During the cooling stage, in contrast with the results obtained at the heating stage, the extent of E_a diminished from 44.38 to 17.63 (kJ/mol), as the LPSG ratio increased from 25 to 75%, which confirms the low influence of temperature on LPSG conformational changes. This result was consistent with the higher value of E_a for XG (80.24 kJ/mol) than LPSG (61.61 kJ/mol) obtained at the cooling stage.

The thermodynamic characteristics of Gibbs free energy, enthalpy and entropy of LPSG-XG mixtures at 25 °C are represented in Table 7. As it can be observed, the ΔG° of all LPSG-XG samples is positive and this characteristic enhanced, at both heating/cooling stages, as the ratio of XG in the mixture increased. In other words, the thermodynamic incompatibility of the mixed system decreases with an increase of LPSG fraction. One of the main reasons for this result may be the higher molecular weight of XG (2×10^6 Da) than LPSG (2.34×10^5 Da), which results in a higher tendency to aggregate and phase separate in systems containing higher XG ratio.

Low entropy of macromolecules mixing indicates more thermodynamic incompatibility between them [70]. The results of entropy obtained based on Eq. (7) for LPSG-XG blends revealed negative values, which diminished with a raise in ratio of XG. It means that the LPSG chains have access to lower extent of the volume occupied by the XG molecules in the high-ratio XG blends (LPSG25-XG75) than that of XG in the low-ratio XG blends

Table 7 The activation energy of complex modulus (E_a), standard Gibbs free energy change (ΔG°), entropy change (ΔS), enthalpy change (ΔH) calculated for the different ratios of LPSG-XG blends during heating/cooling stages at 25°C^a

LPSG-XG (%)	Temperature sweep stage	E_a (kJ/mol)	ΔG° (J/mol)	ΔS (J/mol. $^\circ$ K)	ΔH (J/mol)
LPSG0-XG100	Heating	19.56	–	–	–
	Cooling	80.24	–	–	–
LPSG25-XG75	Heating	9.77	3256.56	– 0.38	3144.20
	Cooling	44.38	2925.73	– 0.56	2759.66
LPSG50-XG50	Heating	12.13	1775.23	– 0.28	1693.09
	Cooling	15.97	961.89	– 0.47	822.47
LPSG75-XG25	Heating	16.32	1227.33	– 0.23	1159.44
	Cooling	17.63	805.44	– 0.36	700.15
LPSG100-XG0	Heating	85.57	–	–	–
	Cooling	61.61	–	–	–

^a LPSG *Lepidium perfoliatum* seed gum, XG xanthan gum

(LPSG75-XG25) at 25 °C; therefore, at increasing XG ratio, ΔS of the systems decreased, which confirms more aggregation of XG due to its higher rigidity at low temperature [32]. The enthalpy of mixing (ΔH) determined by the Eq. (8) showed strongly endothermic values for all the blends that decreased with the increase of LPSG ratio during heating/cooling steps. The value of ΔH points the miscibility or immiscibility of a system, so as the system with negative values have shown miscibility [71]. Accordingly, the results confirmed higher immiscibility of LPSG-XG system at higher XG ratio.

Stiffness characteristics

In this work, the values of Friedrich and Heymann [35] model parameters, shown as A_α and α , which are, respectively, in association with the strength of network and the number of interactions between the experimented hydrocolloids in the given mixing ratios were estimated ($R^2 \geq 0.99$) in the frequency range of 0.0628 to 62.823 rad/s (Table 3). As the results show, the magnitudes of A_α decreases as the LPSG fraction in the blends increases (except for LPSG75-XG25 compared to LPSG50-XG50). As a result, it can be deduced that the highest and the lowest molecular binding exist in the individual dispersions of XG and LPSG, respectively.

The value of the order of relaxation function (α), which is an indication of the 3D structural of the dispersions and it able to identify the network extension [72], was found to be the least for XG (0.14), while no significant difference was obtained among the blends ($p > 0.05$).

The A_α obtained for LPSG (5.88 Pa.rad^{- α} .s ^{α}) was lower than that of sage seed gum (10.06 Pa.rad^{- α} .s ^{α}), but higher than that of guar gum (3.55 Pa.rad^{- α} .s ^{α}), and in the case of α parameter, the value for LPSG (0.16) was lower than the reported values of sage seed gum (0.22) and guar gum (0.52) [73]. Moreover, the values of the former parameter for LPSG-XG blends found to be higher than those for sage seed gum-guar gum and sage seed gum-xanthan gum blends, while for the later parameter, the values were lower than those for sage seed gum-guar gum blends, but almost similar to those of sage seed gum-xanthan gum blends [26, 73].

Synergistic interaction

In this work, the LPSG-XG blends behaviour, antagonism/synergism influences, was studied using Cole-Cole plot, which represents the relationship between the imaginary viscosity (η'') and dynamic viscosity (η'). Cole-Cole plot method is a well-known empirical method applied to analyse the miscibility of polymer blends. As the shape of plotted curves is a smooth, semi-circular shape, it indicates good miscibility, while any deviation from this shape implies a heterogeneous

dispersion and a poorer compatibility of the blends constituents. Figure 8 shows the Cole-Cole plot attained for the LPSG25-XG75, LPSG50-XG50 and LPSG75-XG25 blend samples. As it can be seen, the most semi-circular shape which indicates the greatest compatibility between LPSG and XG was obtained at ratio of 75:25 (power-law index (β)=0.87), while the worst miscibility (poorer compatibility) was shown for the ratio of 25:75 (β =1.02). This finding also was confirmed based on the value of α calculated (Eq. (14)) for the rheological parameters of G' (-0.095), $\tan \delta_{LVE}$ (-0.158), $\tan \delta$ (-0.037) and k (0.101) correspond to the LPSG75-XG25 sample, indicating more synergistic behaviour and lower antagonistic interaction between LPSG and XG at the ratio of 75:25.

Conclusions

This study was dealt with the rheological (viscoelasticity, flow behaviour and thixotropy measurements) and thermo-rheological properties of the blends of *Lepidium perfoliatum* seed gum and xanthan gum to find out their interaction at various ratios. In the LVE, the XG-rich blends exhibited stronger gel structure and greater yield stress values, but lower values of stress at the flow point. Shear-thinning behaviour was observed for XG and LPSG individual gels as well as their blends in steady and oscillatory shear, which comes from weak gel structure formed by overlapping and entanglements of flexible random coil chains. Moreover, the frequency dependant of the samples confirmed weak gel structure, which was not significantly influenced by the ratio of LPSG-XG blends. The weaker gel structure obtained for LPSG-rich blends resulted in a greater departure from Cox-Merz rule. Higher incorporation of LPSG in the blends decreased the thixotropic behaviour as well as recovery parameter (R , %) obtained from in-shear structural recovery test. The steady and dynamic yield stress values attained for LPSG75-XG25 show no significant difference ($p > 0.05$) with those of XG. Higher aggregation probability and more tendency to phase separation in the XG-rich

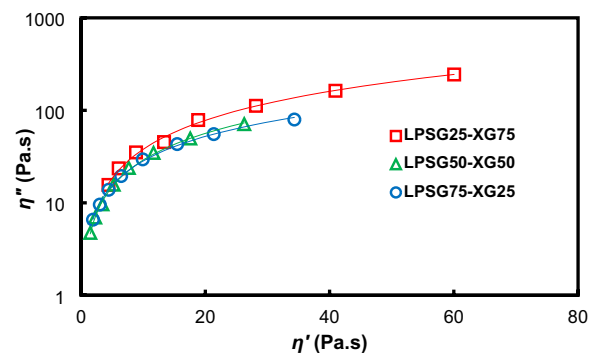


Fig. 8 The Cole-Cole plot of different ratios of LPSG-XG blends; LPSG *Lepidium perfoliatum* seed gum, XG xanthan gum

system (LPSG25-XG75) resulted in more thermodynamic incompatibility (higher ΔG°), which also was confirmed by the value of $\beta = 1.02$ calculated from Cole–Cole plot. Accordingly, the most miscibility and the strongest interaction between LPSG and XG were found at the blend ratio of 75% and 25%, respectively. The method of rheological study used and the results reported in this work can shed light on the interaction behaviour of any carbohydrate-based hydrocolloid blends.

Acknowledgements

The authors would like to appreciate the facilities provided by Laboratoire Rhéologie et Procédés (LRP), Université Grenoble Alpes, France, for performing the rheological experiments.

Author contributions

AY contributed to conceptualization and writing—original draft preparation; AY and KA were involved in methodology, data curation and supervision; GH and SK provided software; AY, SK and GH performed investigation. All authors read and approved the final manuscript.

Funding

No funding.

Availability of data and materials

All data generated or analysed during this study are available from the corresponding author on reasonable request.

Declarations

Ethics approval and consent to participate

This study does not involve any human or animal testing.

Consent for publication

Not applicable.

Competing interests

The authors declare that they do not have any competing interests.

Author details

¹Department of Chemical Engineering, Faculty of Engineering, University of Bonab, East Azerbaijan, Velayat Highway, Bonab 55517-61167, Iran. ²UGA, CNRS, LRP, 363, Rue de la Chimie, Saint-Martin-d'Hères, 38400 Grenoble, France.

Received: 5 November 2022 Accepted: 18 January 2023

Published online: 31 January 2023

References

- Dehghan B, Esmailzadeh Kenari R, Raftani AZ. Nano-encapsulation of orange peel essential oil in native gums (*Lepidium sativum* and *Lepidium perfoliatum*): Improving oxidative stability of soybean oil. *J Food Process Preserv.* 2020;44(11):e14889.
- Yousefi A, Ako K. Controlling the rheological properties of wheat starch gels using *Lepidium perfoliatum* seed gum in steady and dynamic shear. *Int J Biol Macromol.* 2020;143:928–36.
- Koocheki A, Hesarinejad MA, Mozafari MR. *Lepidium perfoliatum* seed gum: investigation of monosaccharide composition, antioxidant activity and rheological behavior in presence of salts. *Chem Biol Technol Agric.* 2022;9(1):61.
- Koocheki A, Taherian AR, Razavi SM, Bostan A. Response surface methodology for optimization of extraction yield, viscosity, hue and emulsion stability of mucilage extracted from *Lepidium perfoliatum* seeds. *Food Hydrocoll.* 2009;23(8):2369–79.
- Yousefi A, Elmarhoum S, Khodabakhshaghdam S, Ako K, Hosseinzadeh G. Study on the impact of temperature, salts, sugars and pH on dilute solution properties of *Lepidium perfoliatum* seed gum. *Food Sci Nutr.* 2022;10(11):3955–68.
- Koocheki A, Taherian AR, Bostan A. Studies on the steady shear flow behavior and functional properties of *Lepidium perfoliatum* seed gum. *Food Res Int.* 2013;50(1):446–56.
- Hesarinejad MA, Koocheki A, Razavi SMA. Dynamic rheological properties of *Lepidium perfoliatum* seed gum: effect of concentration, temperature and heating/cooling rate. *Food Hydrocoll.* 2014;35:583–9.
- Vianna-Filho RP, Petkowicz CLO, Silveira JLM. Rheological characterization of O/W emulsions incorporated with neutral and charged polysaccharides. *Carbohydr Polym.* 2013;93(1):266–72.
- Garcia-Ochoa F, Santos V, Casas J, Gómez E. Xanthan gum: production, recovery, and properties. *Biotechnol Adv.* 2000;18(7):549–79.
- Renou F, Petibon O, Malhiac C, Grisel M. Effect of xanthan structure on its interaction with locust bean gum: toward prediction of rheological properties. *Food Hydrocoll.* 2013;32(2):331–40.
- Kang KS, Pettitt DJ. Xanthan, gellan, wellan, and rhaman. In: Whistler RL, Bemiller JN, editors. *Industrial gums*. New York: Academic Press; 1993. p. 341–98.
- Urlacher B, Noble O. Xanthan. In: Imeson A, editor. *Thickening and gelling agents for food*. London: Chapman & Hall; 1997. p. 284–311.
- Choi HM, Yoo B. Steady and dynamic shear rheology of sweet potato starch–xanthan gum mixtures. *Food Chem.* 2009;116(3):638–43.
- Achayuthakan P, Supphantharika M, Rao M. Yield stress components of waxy corn starch–xanthan mixtures: effect of xanthan concentration and different starches. *Carbohydr Polym.* 2006;65(4):469–78.
- Choppe E, Puaud F, Nicolai T, Benyahia L. Rheology of xanthan solutions as a function of temperature, concentration and ionic strength. *Carbohydr Polym.* 2010;82(4):1228–35.
- Milas M, Rinaudo M, Knipper M, Schuppiser JL. Flow and viscoelastic properties of xanthan gum solutions. *Macromolecules.* 1990;23(9):2506–11.
- Casas JA, Mohedano AF, García-Ochoa F. Viscosity of guar gum and xanthan/guar gum mixture solutions. *J Sci Food Agric.* 2000;80(12):1722–7.
- Abbaszadeh A, Macnaughtan W, Sworn G, Foster TJ. New insights into xanthan synergistic interactions with konjac glucomannan: a novel interaction mechanism proposal. *Carbohydr Polym.* 2016;144:168–77.
- Paradossi G, Chiessi E, Barbiroli A, Fessas D. Xanthan and glucomannan mixtures: synergistic interactions and gelation. *Biomacromol.* 2002;3(3):498–504.
- Mirzaei M, Alimi M, Shokoohi S, Golchoobi L. Synergistic interactions between konjac-mannan and xanthan/tragacanth gums in tomato ketchup: physical, rheological, and textural properties. *J Texture Stud.* 2018;49(6):586–94.
- Kurt A, Toker OS, Tornuk F. Effect of xanthan and locust bean gum synergistic interaction on characteristics of biodegradable edible film. *Int J Biol Macromol.* 2017;102:1035–44.
- Jiang M, Hong Y, Gu Z, Cheng L, Li Z, Li C. Effects of acid hydrolysis intensity on the properties of starch/xanthan mixtures. *Int J Biol Macromol.* 2018;106:320–9.
- Yadav K, Yadav BS, Yadav RB, Dangi N. Physicochemical, pasting and rheological properties of colocasia starch as influenced by the addition of guar gum and xanthan gum. *J Food Meas Charact.* 2018;12(4):2666–76.
- Harding SE, Smith IH, Lawson CJ, Gahler RJ, Wood S. Studies on macromolecular interactions in ternary mixtures of konjac glucomannan, xanthan gum and sodium alginate. *Carbohydr Polym.* 2011;83(2):329–38.
- Pongjanyakul T, Puttipatkhachorn S. Xanthan–alginate composite gel beads: molecular interaction and in vitro characterization. *Int J Pharm.* 2007;331(1):61–71.
- Alghooneh A, Razavi SMA, Behrouzian F. Rheological characterization of hydrocolloids interaction: a case study on sage seed gum–xanthan blends. *Food Hydrocoll.* 2017;66:206–15.
- Razavi SM, Alghooneh A. Understanding the physics of hydrocolloids interaction using rheological, thermodynamic and functional properties: a case study on xanthan gum–cress seed gum blend. *Int J Biol Macromol.* 2020;151:1139–53.
- Annable P, Williams P, Nishinari K. Interaction in xanthan–glucomannan mixtures and the influence of electrolyte. *Macromolecules.* 1994;27(15):4204–11.

29. Copetti G, Grassi M, Lapasin R, Pricl S. Synergistic gelation of xanthan gum with locust bean gum: a rheological investigation. *Glycoconj J*. 1997;14(8):951–61.
30. Kitamura S, Takeo K, Kuge T, Stokke BT. Thermally induced conformational transition of double-stranded xanthan in aqueous salt solutions. *Biopolym: Orig Res Biomol*. 1991;31(11):1243–55.
31. Ferry JD. *Viscoelastic properties of polymers*. New York: John Wiley & Sons; 1980.
32. Razavi SM, Alghooneh A, Behrouzian F. Thermo-rheology and thermodynamic analysis of binary biopolymer blend: a case study on sage seed gum-xanthan gum blends. *Food Hydrocoll*. 2018;77:307–21.
33. Özilgen M. Enthalpy-entropy and frequency factor-activation energy compensation relations for diffusion in starch and potato tissue. *Starch-Stärke*. 1993;45(2):48–51.
34. Rhim JW, Nunes R, Jones V, Swartzel K. Determination of kinetic parameters using linearly increasing temperature. *J Food Sci*. 1989;54(2):446–50.
35. Friedrich C, Heymann L. Extension of a model for crosslinking polymer at the gel point. *J Rheol*. 1988;32(3):235–41.
36. Raei M, Rafe A, Shahidi F. Rheological and structural characteristics of whey protein-pectin complex coacervates. *J Food Eng*. 2018;228:25–31.
37. Steffe JF. *Rheological methods in food process engineering*. Dallas: Freeman press; 1996.
38. Mezger T. *The rheology handbook: for users of rotational and oscillatory rheometers*. Nuernberg: European Coatings; 2020.
39. Razi SM, Motamedzadegan A, Shahidi S-A, Rashidinejad A. Steady and dynamic shear rheology as a tool for evaluation of the interactions between egg white albumin and basil seed gum. *Rheol Acta*. 2020. <https://doi.org/10.1007/s00397-020-01198-5>.
40. Mohsin A, Zaman WQ, Guo M, Ahmed W, Khan IM, Niazi S, et al. Xanthan-Curdlan nexus for synthesizing edible food packaging films. *Int J Biol Macromol*. 2020;162:43–9.
41. Mohsin A, Zhang K, Hu J, Tariq M, Zaman WQ, Khan IM, et al. Optimized biosynthesis of xanthan via effective valorization of orange peels using response surface methodology: a kinetic model approach. *Carbohydr Polym*. 2018;181:793–800.
42. Sadeghi F, Koocheki A, Shahidi F. Physical modification of *Lepidium perfoliatum* seed gum using cold atmospheric-pressure plasma treatment. *Food Hydrocoll*. 2021;120:106902.
43. Zhao L, Pan F, Mehmood A, Zhang Y, Hao S, Rehman AU, et al. Protective effect and mechanism of action of xanthan gum on the color stability of black rice anthocyanins in model beverage systems. *Int J Biol Macromol*. 2020;164:3800–7.
44. Yousefi A, Razavi SM. Dynamic rheological properties of wheat starch gels as affected by chemical modification and concentration. *Starch-Stärke*. 2015;67(7–8):567–76.
45. Zameni A, Kashaninejad M, Aalami M, Salehi F. Effect of thermal and freezing treatments on rheological, textural and color properties of basil seed gum. *J Food Sci Technol*. 2015;52(9):5914–21.
46. Rafe A, Masood H. The rheological modeling and effect of temperature on steady shear flow behavior of *Cordia abyssinica* gum. *J Food Process Technol*. 2014;5(3):1.
47. Rubinstein M, Colby RH. *Polymer physics*. New York: Oxford University Press; 2003.
48. Morris ER. Shear-thinning of 'random coil' polysaccharides: Characterization by two parameters from a simple linear plot. *Carbohydr Polym*. 1990;13(1):85–96.
49. Yamul DK, Navarro AS. Effect of hydrocolloids on structural and functional properties of wheat/potato (50/50) flour dough. *Food Struct*. 2020;24:100138.
50. Casas J, García-Ochoa F. Viscosity of solutions of xanthan/locust bean gum mixtures. *J Sci Food Agric*. 1999;79(1):25–31.
51. Busch VM, Delgado JF, Santagapita PR, Wagner JR, Buera MP. Rheological characterization of vinal gum, a galactomannan extracted from *Prosopis ruscifolia* seeds. *Food Hydrocoll*. 2018;74:333–41.
52. Cox W, Merz E. Correlation of dynamic and steady flow viscosities. *J Polym Sci*. 1958;28(118):619–22.
53. Snijkers F, Vlassopoulos D. Appraisal of the Cox-Merz rule for well-characterized entangled linear and branched polymers. *Rheol Acta*. 2014;53(12):935–46.
54. Rochefort WE, Middleman S. Rheology of xanthan gum: salt, temperature, and strain effects in oscillatory and steady shear experiments. *J Rheol*. 1987;31(4):337–69.
55. Lapasin R, Pricl S, Tracanelli P. Rheology of hydroxyethyl guar gum derivatives. *Carbohydr Polym*. 1991;14(4):411–27.
56. da Silva JL, Gonçalves M, Rao M. Viscoelastic behaviour of mixtures of locust bean gum and pectin dispersions. *J Food Eng*. 1993;18(3):211–28.
57. Yoo B, Figueiredo A, Rao M. Rheological properties of mesquite seed gum in steady and dynamic shear. *LWT-Food Sci Technol*. 1994;27(2):151–7.
58. Martín-Alfonso J, Cuadri A, Berta M, Stading M. Relation between concentration and shear-extensional rheology properties of xanthan and guar gum solutions. *Carbohydr Polym*. 2018;181:63–70.
59. Yoo B, Yoo D, Kim Y-R, Lim S-T. Effect of sugar type on rheological properties of high-methoxyl pectin gels. *Food Scie Biotechnol*. 2003;12(3):316–9.
60. Kim C, Yoo B. Rheological properties of rice starch-xanthan gum mixtures. *J Food Eng*. 2006;75(1):120–8.
61. Wang L, Liu H-M, Zhu C-Y, Xie A-J, Ma B-J, Zhang P-Z. Chinese quince seed gum: flow behaviour, thixotropy and viscoelasticity. *Carbohydr Polym*. 2019;209:230–8.
62. Sun A, Gunasekaran S. Yield stress in foods: measurements and applications. *Int J Food Prop*. 2009;12(1):70–101.
63. Dankar I, Haddarah A, El Omar F, Sepulcre F, Pujolà M. Assessing the microstructural and rheological changes induced by food additives on potato puree. *Food Chem*. 2018;240:304–13.
64. Dinkgreve M, Paredes J, Denn MM, Bonn D. On different ways of measuring "the" yield stress. *J Nonnewton Fluid Mech*. 2016;238:233–41.
65. Tabilo-Munizaga G, Barbosa-Cánovas GV. Rheology for the food industry. *J Food Eng*. 2005;67(1–2):147–56.
66. Herschel W, Bulkley R. Measurement of consistency as applied to rubber-benzene solutions. *Am Soc Test Proc*. 1926;26:621–33.
67. Tipvarakarnkoon T, Senge B. Rheological behaviour of gum solutions and their interactions after mixing. *Annu Trans Nordic Rheol Soc*. 2008;16:73–80.
68. Song K-W, Kim Y-S, Chang G-S. Rheology of concentrated xanthan gum solutions: Steady shear flow behavior. *Fibers Polym*. 2006;7(2):129–38.
69. Pourfarzad A, Yousefi A, Ako K. Steady/dynamic rheological characterization and FTIR study on wheat starch-sage seed gum blends. *Food Hydrocoll*. 2021;111:106380.
70. Stephen AM, Phillips GO. Food polysaccharides and their applications. In: Stephen AM, Phillips GO, Williams PA, editors. *Food polysaccharides and their applications*. 2nd ed. London: Taylor and Francis; 2016.
71. Nie H, Liang X, He A. Enthalpy-enhanced Janus nanosheets for trapping nonequilibrium morphology of immiscible polymer blends. *Macromolecules*. 2018;51(7):2615–20.
72. Gabriele D, de Cindio B, D'Antona P. A weak gel model for foods. *Rheol Acta*. 2001;40(2):120–7.
73. Razavi SMA, Alghooneh A, Behrouzian F, Cui SW. Investigation of the interaction between sage seed gum and guar gum: steady and dynamic shear rheology. *Food Hydrocoll*. 2016;60:67–76.

Publisher's Note

Springer Nature remains neutral with regard to jurisdictional claims in published maps and institutional affiliations.

Submit your manuscript to a SpringerOpen® journal and benefit from:

- Convenient online submission
- Rigorous peer review
- Open access: articles freely available online
- High visibility within the field
- Retaining the copyright to your article

Submit your next manuscript at ► [springeropen.com](https://www.springeropen.com)